ChemComm

COMMUNICATION

View Article Online
View Journal | View Issue

Cite this: *Chem. Commun.*, 2017, 53, 12414

Received 25th August 2017,
Accepted 9th October 2017

DOI: 10.1039/c7cc05669a

rsc.li/chemcomm

The active site for the water oxidising anodic iridium oxide probed through *in situ* Raman spectroscopy†

Zoran Pavlovic, Chinmoy Ranjan,* Maurice van Gastel and Robert Schlögl

The structure of anodic iridium oxide (IrO_x) under water oxidation was explored using *in situ* Raman spectroscopy and theoretical calculations. Isotopic substitution experiments and theoretical calculations confirmed formation of an Ir═O species during oxygen evolution reaction.

The oxygen electrode remains a central challenge in implementing a hydrogen-based economy.[1,2] IrO_x remains one of the most important catalysts for water oxidation reaction.[3] Dimensionally stable anodes (DSA) are composed of primarily IrO_2.[4–8] These materials require being treated through activation protocols before they can be implemented. IrO_x materials were shown to be very active by Mallouk *et al.*[9] In the alkaline media, Mallouk *et al.* proposed that these materials are unstable and form molecular species that show oxygen activity.[10] In fact, the activity shown by these materials in alkaline electrolytes was much higher than in acidic or neutral electrolytes. We have recently characterized the active IrO_x material through *ex situ* Raman spectroscopy on anodic IrO_x grown on an iridium foil.[11] Attempts to understand the mechanism of OER on IrO_x has encouraged operando studies using XPS and XAS.[12,13] These investigations focused on an Ir-centered approach to understanding the nature of the active catalyst. XPS studies observed an additional Ir 4f peak at higher binding energy (+0.7 eV) during OER and suggested an Ir^{5+} species forming during the catalytic event.[12] Minguzzi *et al.* suggested the formation of both Ir^{3+} and Ir^{5+} during OER. But both these studies do not compare the shifts to standard Ir-containing compounds. High oxidation states (+5 or greater) are only known for fluorine-containing molecules amongst the stable Ir compounds or in IrO_x molecular species isolated within a noble gas matrix. Reier *et al.* and Pfeiffer *et al.* observed an additional feature at 529 eV in the O-Kedge NEXAFS spectra of highly OER active Ir–NiO_x and amorphous IrO_x respectively. Using DFT calculations, they have suggested this to be an electrophilic oxygen species present in these materials.[14–16] By the nature of their inquiry, these studies cannot clarify the exact chemical nature of the IrO_x active site which is possible through vibrational spectroscopy. Mo *et al.* carried out *in situ* Raman spectroscopy on IrO_x/Au system but essentially used XAS data for interpretation of results.[17] Frei and coworkers have investigated IrO_x clusters as OER catalysts using rapid scan FTIR under visible light.[18] They reported detection of a transient Ir–OOH species with O–O vibration being detected at 830 cm^{-1}. This work goes beyond work reported by Pavlovic *et al.* and uses *in situ* Raman spectroscopy to understand the behavior of these materials under conditions of OER.[11] Specifically we focus on active site that forms *in situ*. We suggest a Ir═O species, with five coordinated square pyramidal Ir as the active site for water oxidation and suggest a mechanistic pathway for product formation and replenishment of the active site.

Cyclic voltammogram of IrO_x materials in different electrolytes is well known (Fig. S1, ESI†). All the potentials reported in this paper are referenced to the reversible hydrogen electrode (RHE). The material was electroprecipitated at 1.5 V onto a Au substrate as shown by Mallouk *et al.*[9] In our previous publication we have shown that the anodic Iridium oxide is essentially a hydrous material with OH and H_2O groups playing important role in its overall structure.[11] Experiments of IrO_x/Au were conducted in an *in situ* Raman cell, using Biologic VSP-300 potentiostat. Raman spectra were collected with Ocean Optics QE65 pro spectrometer using 785 nm Laser source. The Laser intensity was maintained at 500 mW per 0.1 mm^2 at the sample (collection time of 10 s). The potential was scanned from 0.4–1.8 V, at steps of 0.1 V.

Results of the *in situ* Raman experiment are shown in Fig. 1. More details of the experiments are provided in the ESI.† Peaks at 225 and 324 cm^{-1} originate from the Au surface. The peaks from 450–780 cm^{-1} originate from iridium oxygen vibrations, where peak assignments have been used from Pavlovic *et al.*[11] Electrochemically, four regions (R) in the IrO_x CV can be clearly

Department of Heterogeneous Catalysis, Max Planck Institute for Chemical Energy Conversion, Stiftstrasse 34-36, Muelheim and Ruhr, 45470, Germany.
E-mail: chinmoy.ranjan@cec.mpg.de

† Electronic supplementary information (ESI) available: Experimental details, cyclic voltammograms, Raman spectra in various electrochemical media and computational details. See DOI: 10.1039/c7cc05669a

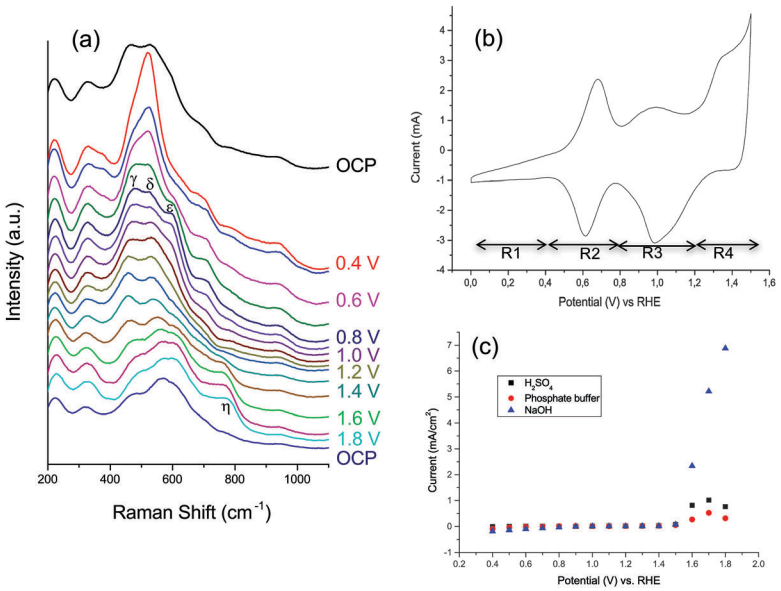

Fig. 1 (a) *In situ* Raman spectroscopy of IrO_x/Au system in 0.1 M NaOH. The peaks labeled by greek letters originate from Ir–O stretch vibrations. Rest of the peaks can be assigned to Au substrate (ESI,† Section 2). η peak is only visible during the process of OER and disappears with removal of applied potential. Peak assignments (in greek letters) have been borrowed from Pavlovic *et al.*[11] (b) CV of IrO_x/Au in 0.1 M NaOH (c) Average currents from *in situ* experiments in various electrochemical media.

identified. R1($E < 0.4$ V), R2 ($0.4 < E < 0.7$ V), R3 ($0.7 < E < 1.2$ V) and R4 ($E < 1.4$ V). Whereas R1 corresponds to a colorless compound rich in Ir^{3+}, R2 represents the region of first oxidation wave from $Ir^{3+} \leftrightarrow Ir^{4+}$. At the beginning of the experiment at OCP, there is a certain peak structure (465, 527, 600, 702 cm^{-1}), which can be attributed to the Ir–O–Ir stretch vibrations of μ-oxo type from the basal plane of edge sharing IrO_6 octahedra.[11] As soon as the potential of 0.4 V is applied, a sharp peak at 520 cm^{-1} is formed. This is the most dominant peak δ in region R1. Region R1 has no ε peak which appears in R2. The ε peak loses intensity in R3. R4 shows significant drift of peaks $\gamma \rightarrow \varepsilon$ towards higher frequencies. At potentials 1.3 V and higher, AuO_x is formed (Fig. S4, ESI†). Thus peaks in R4 have substantial AuO_x contribution to them. The final peaks observed at OCP in the treated materials are composed of both IrO_x and AuO_x peaks. The peak η at 771 cm^{-1} is seen in R4. This peak disappears as soon as the applied potential is switched off. This peak does not exist in experiments done on a bare Au surface and thus must be assigned to IrO_x material under conditions of water oxidation. Isotopic substitution using D_2O and H_2O^{18} as synthesis and reaction media were also carried out. Results have been tabulated in Table 1. Fig. 2 shows effects of isotopic substitution on η. In the experiment that has 50 : 50 ($H_2O : H_2O^{18}$), only two peaks of nearly equal intensity were visible. Thus this peak could be assigned to Ir═O vibration (as opposed to any other species that contained O–O, or OH vibration). If O movement is the primary oscillator in this vibration, then one can expect a shift of $\Delta f \sim \sqrt{8/9} \sim 45\ cm^{-1}$ upon O^{18} substitution. Deuterium substitution resulted in almost no shift of the peak ($\Delta f \sim 5\ cm^{-1}$). For Ir–O–OH containing groups, the shift reported by Frei *et al.* due to deuteration was 30 cm^{-1}.[18] Small shifts due to deuteration are possible through altered hydrogen bonding contributions from the solvent. Vibrations where the motion of the hydrogen atom explicitly contribute to the vibrational mode show significant alteration of frequency upon deuteration due to the large mass

Table 1 Peaks obtained in the Raman spectra of IrO_x/Au labeled at 0.8 V. The peaks tend to move with applied potential and thus their exact location can be described only at a certain potential. The Ir–O stretching assignments have been borrowed from Pavolovic *et al.*[11]

Peak labels	H_2O	D_2O	H_2O^{18}	1 : 1 ($H_2O : H_2O^{18}$)	H_2O^{18} tested in H_2O
γ	476	475	423	454, 482	430, 458, 480
δ	527	554	476	541, 482	554
ε	595	602	554	605, 552	608
η[a]	771	767	712	722, 771	—

[a] Collected at 1.7 V.

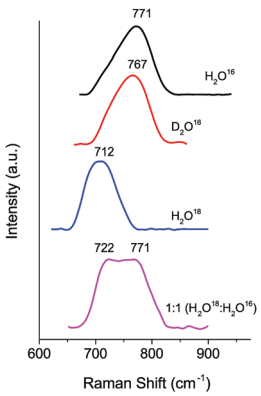

Fig. 2 Raman spectra of the η peak in various isotopically labeled electrolytes. The peaks are background corrected and normalized (details in Experimental section).

change $f_D/f_H \sim 1\sqrt{2}$. Fig. S5 (ESI†) shows the results from various experiments with combinations of H_2O, D_2O, and H_2O^{18} containing electrolytes. Fig. 2, shows η peak at OER potentials in variously labeled electrolytes. Fig. S5(d) (ESI†) shows the results of experiments when material was synthesized in H_2O^{18} and tested in H_2O.[16] Peaks γ to ε begin to split into two sets of peaks in the beginning of R3 indicating that material exchanges oxygens with the electrolyte even at potentials as low as 0.7 V. Even the position of η peak only shows the contribution from O^{16} isotope.

Theoretical calculations using density functional theory were carried out to better understand the IrO_x system (Fig. S6–S8, ESI†). Specifically, calculations were performed to understand the identity of the Ir=O species. A trimeric IrO_6 unit was used to construct a model system for calculation. It was found that an Ir–O unit on the central Ir atom resulted in the formation of a square pyramidal central Ir atom. [Ir^{4+}–Ir^{4+}–Ir^{4+}] trimeric IrO_x cluster was used for computation (Fig. 3). The Ir–O vibration was computed to be at 829 cm^{-1}. Furthermore it was found that the vibrations could be significantly modulated through hydrogen bonding near the "Ir–O" *e.g.* the Ir–O vibration was reduced to 766 cm^{-1} from 829 cm^{-1} by placing a H_2O molecule near the Ir–O moiety. Besides, the relative intensity of this vibration was found to be very strong compared to the other vibrations within this molecule. We believe at the optimum potential some of the $[IrO_6]_n$ species turn into the OER active Ir=O species that removes any further oxidative strain from the material. Even though present in much less quantity, the extremely high Raman activity of the Ir–O stretch vibration makes it possible for the active species to be detected within a matrix of $[IrO_6]_n$ containing material. The 771 cm^{-1} peak can also be detected in acidic media but has a much smaller intensity (the OER activity of the material in acidic and neutral media is much less than alkaline media (Fig. S2, ESI†)). This is likely because the material is highly condensed in the acidic and neutral media and not many exposed active sites containing Ir=O species form, which gets reflected in the overall activity of the material. Ir–OOH species (Fig. S7, ESI†) were also computed. The frequency of vibration of O–O stretch was 715 cm^{-1}, besides the O–O stretch Raman intensity was much smaller. In light of our experimental and computational investigations we assign the observed 771 cm^{-1} vibration to Ir=O stretch of a square pyramidal Ir site. The frontier orbitals of IrO_x were calculated and have been visualized in Fig. 3. The SOMO (Fig. 3(b)) shows that Ir–O unit is the most reactive part of the molecule with a major part of the molecular orbital localised in this region. The frontier orbitals are anti-bonding in nature between Ir-d and O-p with significant localization on O atom making it a suitable target for reaction. We believe this oxygen may be responsible for making the important O–O bond during the formation of molecular O_2 from water (Fig. 4). M–O species responsible for oxidizing water are common in literature.[19] In case of Mn-containing Photosystem II catalyst, the O–O bond formation either happens through a nucleophilic attack at the Mn–O center (Mn^{5+}–O, Mn^{4+}–O or Mn^{4+}–oxyl) species or by an oxyl–oxyl radical coupling mechanism.[20–22] But the exact nature of the species is debatable. It has been suggested in the literature that an electrophilic oxygen at the active site is essential to make reactions like O–O bond formation and C–H bond activation, possible.[16,23,24] Wang *et al.* and Concepcion and coworkers suggested an O–O bond formation using nucleophilic attack on Ru=O site.[25,26] Using DFT based theory, Mai *et al.* suggested that C–H activation essentially consists of two parts, an Fe^{4+}=O species which was a precursor to Fe^{3+}–$O^{\bullet -}$ oxyl species that carried out the hydrogen atom transfer.[23] Similarly, using DFT calculations Yang *et al.* have argued that Ru^{5+}=O can act as a precursor to Ru^{4+}–$O^{\bullet -}$ oxyl species which carries out water O–O bond formation. For the IrO_x cluster shown in Fig. 3, the total Löwdin charge at the oxygen atom amounts to only −0.12 (as compared to −0.35 for the bridging oxo-s) and the Löwdin spin population at the central Ir and oxo amounts to 47% and 29%, respectively. Semantically, although this charge distribution would be compatible with a metal-oxyl ($O^{\bullet -}$) species, the spin distribution rather indicates a much lower spin population at the oxygen (29%) than expected for a radical species (∼100%). This is the result of a somewhat covalent Ir–O π-interaction that involves the spin carrying d_{xz} orbital (t_{2g} in octahedral symmetry) at Ir (ESI†). We believe what we see in our experiment, is the structure that is precursor to the reactive oxyl species as proposed by Mai and Yang *et al.*[23,24] The observation of a reactive oxyl radical species under experimental conditions remains difficult,

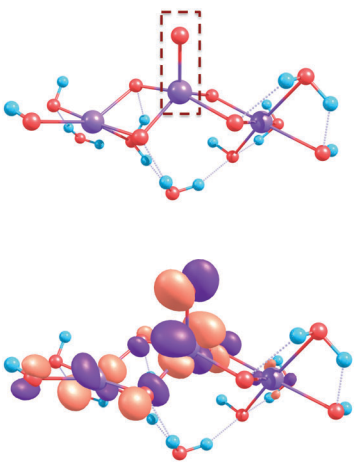

Fig. 3 Theoretical calculations were carried out on IrO_x species containing with "Ir–O" moiety. The calculations resulted in an Ir–O species that was essentially square pyramidal at the Ir center. (Top) Ir^{4+} containing species with the central atom having the Ir–O bond. The oxygen atom has been labeled with a O* (Top). (bottom) SOMO of the species.

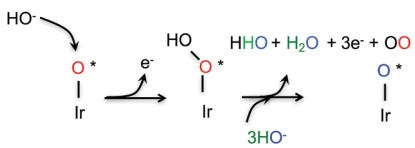

Fig. 4 Proposed active species responsible for water oxidation in IrO_x materials (alkaline media). Suggested mechanism of oxidation of water and regeneration of the active site is shown. The oxo species is likely to go through an oxyl type species before the O–O bond is formed.

specifically at room temperature. Herlihy *et al.* observed an oxyl species on TiO_x system using *in situ* ultrafast infrared spectroscopy.[27] Based on our data, we claim an Ir–O species that can in principle act as a precursor to a highly electrophilic oxyl species that reacts with water (or dissociated water) to form an O–O bond.

The scaffold enabling the OER is derived from a highly hydrous $[IrO_6]_n$ species (of the type $IrO_x(OH)_y(H_2O)_z$), where each Ir atom is octahedrally coordinated by oxygens. Whereas the colour and vibrational spectroscopy of most of this material can be traced using *ex situ* spectroscopy, the formation of an active a square pyramidal ''Ir–O'' species is detectable only through *in situ* spectroscopy under applied potential. We propose that this Ir–O species is the active site within the molecule which is open to attack from H_2O molecules leading to formation of O_2 through formation of an O–O bond as shown in Fig. 4. The OER chemistry is likely to proceed primarily in the ligand sphere.

The authors thank BMWi for supporting this work through grant 03ESP106D (EKOLYSER). Open Access funding provided by the Max Planck Society.

Conflicts of interest

There are no conflicts to declare.

References

1 J. A. Turner, *Science*, 2004, **305**, 972–974.
2 R. Schlögl, *ChemSusChem*, 2010, **3**(2), 209–222.
3 C. C. L. McCrory, S. H. Jung, J. C. Peters and T. F. Jaramillo, *J. Am. Chem. Soc.*, 2013, **135**(45), 16977–16987.
4 A. Hrussanova, E. Guerrini and S. Trasatti, *J. Electroanal. Chem.*, 2004, **564**, 151–157.
5 A. Damjanovic and M. K. Y. Wong, *J. Electrochem. Soc.*, 1967, **114**, 592–593.
6 E. Guerrini, H. Chen and S. Trasatti, *J. Solid. State. Electrochem.*, 2007, **11**, 939–945.
7 S. Trasatti, *Electrochim. Acta*, 1991, **36**, 225–241.
8 S. Trasatti, *Electrodes of Conductive Metallic Oxides, Part A and Part B*, *Elsevier*, *Amsterdam*, 1980–1981.
9 Y. Zhao, N. M. Vargas-Barbosa, E. A. Hernandez-Pagan and T. E. Mallouk, *Small*, 2011, **7**(14), 2087–2093.
10 Y. Zhao, N. M. Vargas-Barbosa, M. E. Strayer, N. S. McCool, Maria-Erini Pandelia, T. P. Saunders, J. R. Swierk, J. F. Callejas, L. Jensen and T. E. Mallouk, *J. Am. Chem. Soc.*, 2015, **137**(27), 8749–8757.
11 Z. Pavlovic, C. Ranjan, Q. Gao, M. van Gastel and R. Schloegl, *ACS Catalysis*, 2016, **6**(12), 8098–8105.
12 H. G. Sanchez Casalongue, M. Ling Ng, S. Kaya, D. Friebel, H. Ogasawara and A. Nilsson, *Angew. Chem., Int. Ed.*, 2014, **53**, 7169–7172.
13 A. Minguzzi, O. Lugaresi, E. Achilli, C. Locatelli, A. Vertova, P. Ghigna and S. Rondinini, *Chem. Sci.*, 2014, **5**, 3591–3597.
14 T. Reier, Z. Pawolek, S. Cherevko, M. Bruns, T. Jones, D. Teschner, S. Selve, A. Bergmann, H. N. Nong, R. Schlögl, K. J. J. Mayrhofer and P. Strasser, *J. Am. Chem. Soc.*, 2015, **137**(40), 13031–13040.
15 T. Reier, H. N. Nong, D. Teschner, R. Schlögl and P. Strasser, *Adv. Energy Mater.*, 2016, 1601275, DOI: 10.1002/aenm.201601275.
16 V. Pfeifer, T. E. Jones, J. J. Velasco Vélez, C. Massué, M. T. Greiner, R. Arrigo, D. Teschner, F. Girgsdies, M. Scherzer, J. Allan, M. Hashagen, G. Weinberg, S. Piccinin, M. Hävecker, A. Knop-Gericke and R. Schlögl, *Phys. Chem. Chem. Phys.*, 2016, **18**, 2292.
17 Y. Mo, I. C. Stefan, W. B. Cai, J. Dong, P. Carey and D. A. Scherson, *J. Phys. Chem. B*, 2002, **106**, 3681–3686.
18 N. Sivasankar, W. W. Weare and H. Frei, *J. Am. Chem. Soc.*, 2011, **133**, 12976.
19 Hohenberger, Johannes, Ray, Kallol, Meyer and Karsten, *Nat. Commun.*, 2012, **3**, 720.
20 N. Cox, D. A. Pantazis, F. Neese and W. Lubitz, *Acc. Chem. Res.*, 2013, **46**, 1588–1596.
21 L. Rapatskiy, *et al.*, *J. Am. Chem. Soc.*, 2012, **134**, 16619–16634.
22 P. E. M. Siegbahn, *Biochim. Biophys. Acta*, 2013, **1827**, 1003–1019.
23 B. K. Mai and Y. Kim, *Inorg. Chem.*, 2016, **55**(8), 3844–3852.
24 X. Yang and M. H. Baik, *J. Am. Chem. Soc.*, 2006, **128**(23), 7476–7485.
25 L. P. Wang, Q. Wu and T. Van Voorhis, *Inorg. Chem.*, 2010, **49**, 4543.
26 J. J. Concepcion, M. K. Tsai, J. T. Muckerman and T. J. Meyer, *J. Am. Chem. Soc.*, 2010, **132**, 1545.
27 D. M. Herlihy, M. M. Waegele, X. Chen, C. D. Pemmaraju, D. Prendergast and T. Cuk, *Nat. Chem.*, 2016, **8**, 549–555.